Characterization of Composite Microstructure and Damage Using Optical Coherence Tomography

Joy P. Dunkers, Carl G. Zimba, Kathleen M. Flynn, and Donald L. Hunston
Polymers Division
National Institute of Standards and Technology
Gaithersburg, MD 20899-8543

Rohit Prasankumar, Xingde Li and James G. Fujimoto
Department of Electrical Engineering and Computer Science and
Research Laboratory of Electronics
Massachusetts Institute of Technology
Cambridge, MA 02139

ABSTRACT

Optical coherence tomography (OCT) is a non-destructive and non-contact technique that images microstructure within scattering media. In this work, the versatility of OCT for non-destructive evaluation is demonstrated through imaging of composite microstructure and damage. Imaging of composite microstructure is demonstrated through tomographic reconstructions of an epoxy/unidirectional E-glass composite and an epoxy/0-90° woven E-glass composite. Imaging of damage is shown by tomographic reconstruction of impact damage in a epoxy/unidirectional E-glass composite. The volumetric reconstruction of the composite is re-sliced along the thickness axis to reveal the propagation of cracks though the reinforcement layers. Advantages and limitations of OCT are discussed.

Keywords: Optical coherence tomography, composites, microstructure, damage.

1. INTRODUCTION

In the past, microstructure and damage in polymer matrix composites have often been characterized using destructive techniques such as microscopy on sectioned samples which provide detailed information on a small size scale. The capability to measure these features non-destructively, however, is very desirable since that permits monitoring of damage evolution and correlation of the results with microstructural features that can initiate, influence, or even control the damage. It is even more advantageous if these measurements are performed with a single technique because this eliminates the complications involved in combining data from different sources. Optical coherence tomography (OCT) is a new measurement method that can characterize both microstructure and damage with high resolution and good penetration depth.

Optical coherence tomography is a non-invasive, non-contact optical imaging technique that allows the visualization of microstructure within scattering media [1,2,3]. OCT uses light in a manner analogous to the way ultrasound imaging uses sound, providing significantly higher spatial resolution (10 μm to 20 μm) albeit with shallower penetration depth. OCT is based upon low-coherence optical ranging techniques where the optical distance to individual sites within the sample is determined by the difference in time, relative to a reference light beam, for an incident light beam to penetrate and backscatter within the sample. This temporal delay is probed using a fiber optic interferometer and a broadband laser light source. The fiber optic interferometer consists of single-mode optical fiber coupled with a 50/50 fiber optic splitter that illuminates both the sample and a linearly translating reference mirror. Light reflected from the reference mirror recombines with light back-scattered and reflected from the sample at the 50/50 splitter to create a temporal interference pattern which is measured with a photodiode detector. The resulting interference patterns are present only when the optical path difference of the reference arm matches that of the sample arm to within the coherence length of the source. The incident light beam is scanned and repeated measurements are performed at different transverse positions to generate a two dimensional array which represents the backscattering or backreflection of a cross sectional plane of the material. This data can be displayed as a grey scale or false color image.

The axial, or z, spatial resolution that can be obtained with OCT is determined by the coherence length, or inverse spectral width, of the light source and is typically 10 μm to 20 μm (Figure 1). The light source is typically a superluminescent diode laser, with a resolution as low as 10 μm to 15 μm. Femtosecond laser sources have also been used to achieve higher resolutions of <5 μm and imaging speeds of several frames per second [4,5]. The transverse, or x, spatial resolution of OCT is determined by the focal spot size on the sample, which is typically 10 μm to 30 μm. The ultimate limitation on the depth of penetration within the sample is the attenuation of light caused by scattering and is nominally a few millimeters. Three-dimensional images of the sample are obtained by rastering the sample in the x direction between successive OCT measurements along the y-axis.

OCT as a non-destructive evaluation (NDE) tool compares very favorably to more established composite NDE techniques. Both transducer and laser based ultrasonics have been used for NDE of polymer composites. Their practical resolution is on the order of 1 mm with tens of millimeters in penetration depth[6,7]. A major drawback to ultrasonics is that the depth of a feature must be determined by model studies, whereas, it is known precisely using OCT. However, ultrasonic testing can evaluate carbon fiber composites, which OCT cannot since it is an optical technique. Both OCT and ultrasonics suffer from contrast degradation and shadowing through the sample thickness. Two x-ray based techniques have been studied. X-ray radiometry is the more established technique, with a spatial resolution of hundreds of microns and tens of millimeters in penetration depth[8]. The main drawback in performing x-ray radiometry is that a dye penetrant must be used for contrast. A method more recently applied to composites, x-ray computed tomography, has a similar resolution and penetration to its counterpart. The accuracy of the x-ray attenuation, and thereby the feature intensity and position, is a complex function of many variables, and additional constraints complicate image interpretation[9]. Nuclear magnetic resonance imaging can reach the spatial resolution of OCT, but is limited to imaging only highly mobile species such as water or plasticizers[10]. When considering NDE techniques for microstructure evaluation, OCT offers an excellent combination of spatial resolution, depth of field, and imaging accuracy.

In this work, the potential of OCT for imaging both microstructure and damage is demonstrated. The fiber architectures of an epoxy/unidirectional E-glass composite and an epoxy/0-90° woven E-glass composite are shown through volumetric imaging. The impact of the microstructure on permeability and mechanical performance predictions is discussed. OCT imaging of composite damage is shown by a tomographic reconstruction and re-slicing of impact damage along the thickness of the composite. This re-slicing of the image data reveals the progression of cracking and delamination within the composite.

2. EXPERIMENTAL

2.1 Materials

The epoxy resin systems consisted of a diglycidyl ether of bisphenol A (DGEBA) monomer (Tactix123, Dow Chemical Company, Midland, MI) and two amines[11]. Aromatic methylene dianiline (MDA) and aliphatic poly(propylene glycol)bis(2-aminopropyl ether) (Jeffamine D400) ($M_{r,n} \approx 400$) were purchased and used as received from Aldrich (Minneapolis, MN). The oxirane/ amine stoichiometry was 2 mol oxirane/1 mol amine. The amine composition consisted of 0.07 mol MDA and 0.93 mol D400. Details of the mixing and resin transfer molding are provided elsewhere[12]. The refractive index of the postcured resin and of the fibers is 1.552±0.004 and 1.554±0.004, respectively, as measured by white light and index matching fluids. The fiber volume fraction for the epoxy/unidirectional E-glass composite is 44 % and 46 % for the epoxy/ 0-90° woven E-glass composite.

2.2 Instrumentation

The imaging system used in this study is schematically shown in Figure 1. A commercial superluminescent light source (AFC Technologies Inc., Hull, Quebec, Canada) was used for the work reported here. The source operated at 1.3 μm with an output power of up to 15 mW and a spectral bandwidth of 40 nm, corresponding to an axial spatial resolution of ≈20 μm. The laser light was coupled into a single-mode fiber-optic Michelson interferometer and delivered to both the reference mirror and the sample. The reference mirror was mounted on a rotating galvanometer, which was driven with a sawtooth voltage waveform. Transverse scanning was performed using a computer controlled motorized stage to translate the sample.

The interferometric signal was electronically filtered with a bandpass centered on the fringe or heterodyne frequency. The filtered fringe waveform was then demodulated, digitized and stored on a computer. The high dynamic range of this system allowed back-reflections as weak as femtowatts of power to be detected. Images were displayed by mapping the logarithm of the signal strength to a gray scale look-up table. The acquisition time for each image was approximately 1 min. The axial (y) measurement range was determined by the distance the reference mirror moves (4.5 mm) normalized by the refractive index (n) of the sample: 4.5 mm/n. The probe beam was focused to a 30 μm diameter spot at a depth of approximately 750 μm to 1000 μm below the surface of the sample.

3. RESULTS AND DISCUSSION

The OCT image of the epoxy/unidirectional E-glass composite is shown in Figure 2A. The composite cross-section is shown along the x-z plane. The image dimensions are 6.00 mm along the x axis, 1.48 mm along the z axis, and 3.85 mm axis the y axis. The gray ellipses are the fiber tows which are approximately 2 mm wide and 750 μm thick and consist of about two thousand, 10-20 μm diameter glass fibers[13]. The long axis of the tows is shown on the x-y plane. The polyester stitching that holds a single layer of tows together is indicated by the black arrows. Upon closer inspection, small dark areas are evident inside the fiber tows. These dark areas are high reflectivity regions indicative of individual voids. During the molding process, air can become entrapped as channels in tows if there is insufficient driving pressure, high resin viscosity or low reinforcement permeability[14]. Re-slicing of the volumetric information along an x-y plane at a depth of z has revealed these voids in the fiber tows[15]. Also, the OCT images provide important information about the permeability of the reinforcement since the stacking of the layers has a large influence on the infiltration of the resin with the reinforcement. A preform with the tows in a nested configuration has about a 50 % lower permeability than the same material with the tows in a stacked configuration[13,16].

The volumetric reconstruction of the epoxy/0-90° woven composite is shown in figure 2B. In this image, tows that run along the x axis travel above and below the tows that are found along the y axis. The image dimensions are 6.14 mm along the x axis, 2.13 mm along the z axis, and 4.95 mm along the y axis. Arrow 1 identifies the tows along the x axis that are crossing over the tows along the y axis. Arrow 2 shows the tows along the y axis that are crossing over the tows along the x axis. The layer microstructure has a direct influence on mechanical properties and has been studied elsewhere[17].

OCT has also been used for non-destructive evaluation of damage in the composites. To illustrate this, the epoxy/uni-directional E-glass composite was subjected to impact damage, and imaging was performed along a surface crack that was impacted. Figures 3A through 7A show the damage along the x-y plane through the first layer of composite and are all 5.50 mm wide and 1.98 mm high. Figures 3B through 7B are y-z images showing the position of the tows designated by the dark colored crossing thread and are all 1.98 mm wide (y axis) and 2.23 mm high (z axis). The arrow on the left of these figures indicates the position of the image in figures 3A through 7A with respect to the tow placement.

The damage at the surface of the composite is shown in figure 3A by the arrow, which points to the ridge created by the impact. Figure 4A shows a slice of the composite 337 μm below the surface. The black lines are drawn into this and subsequent figures to indicate the path of the tows. Arrows 1 and 2 point to crack propagating through the fiber tow. Arrow 3 shows the polyester crossing threads that hold the top layer together. Figure 5 shows images that are 460 μm from the surface. The crack indicated by arrow 1 is beginning to propagate along the tow and resin boundary. It is about 820 μm long and is shown to be approaching the bottom of the tow in figure 5B. The crack extends to 1.8 mm long in figure 6A that is 550 μm from the surface as shown by arrow 1. The polyester stitching is still evident (arrow 2). Finally, a delamination zone is shown by the white arrow in Figure 7A at the interface between the bottom of the first tow layer and resin (Figure 7B). The delamination is about 1.9 mm wide and 0.50 mm high and 652 μm from the surface. This crack continues to propagate into the second layer, and a delamination area is found at 1.66 mm down as well. Damage in the direction of the tows is consistent with impact damage observed in other composites[18]. To summarize, the crack created from the impact damage at the surface of the composite propagates through the glass tow. About two thirds of the way through the tow, a crack at the tow and resin boundary begins to propagate along the tow. This crack continues to lengthen and widen until the bottom of the tow is reached and the delamination area shown in Figure 7A is found. Then, the crack continues into the second layer of tows until another delamination area is created at 1.66 mm below the surface.

ACKNOWLEDGEMENTS

REFERENCES

[1] D. Huang, E. A. Swanson, C. P. Lin, J. S. Schuman, W. G. Stinson, W. Chang, M. R. Hee, T. G. Flotte, C. A. Puliafito, and J. G. Fujimoto, "Optical coherence tomography," *Science* **254**, pp. 1178-1181, 1991.

[2] J. G. Fujimoto, M. E. Brezinski, G. J. Tearney, S. A. Boppart, B. Bouma, M. R. Hee, J. F. Southern, and E. A. Swanson, "Optical biopsy and imaging using optical coherence tomography," *Nature Medicine* **1**, pp. 970-972, 1995.

[3] M. Bashkansky, M. D. Duncan, M. Kahn, D. Lewis, J. Reintjes, "Subsurface defect detection in ceramics by high-speed high-resolution optical coherent tomography," *Opt. Lett*. **22**, p. 61, 1997.

[4] B. Bouma, G. J. Tearney, S. A. Boppart, M. R. Hee, M. E. Brezinski, and J. G. Fujimoto, "High resolution optical coherence tomographic imaging using a modelocked Ti:Al$_2$O$_3$ laser source," *Opt. Lett*. **20**, pp. 1-3, 1995.

[5] G. J. Tearney, B. E. Bouma, S. A. Boppart, B. Golubovic, E. A. Swanson, and J. G. Fujimoto, "Rapid Acquisition of in vivo biological images using optical coherence tomography," *Opt. Lett*. **21**, pp. 1408-1410, 1996.

[6] S. Wooh and I. Daniel, "Three-dimensional ultrasonic imaging of defects and damage in composite materials," *Materials Evaluation*, **48(5)**, pp. 1206-1199, 1994.

[7] R. J. Dewhurst, R. He, and Q. Shan, "Defect visualization in carbon fiber composite using laser ultrasound," *Materials Evaluation*, **51(8)**, pp. 935-940, 1993.

[8] A. L. Highsmith and S. Keshav, "Quantitative assessment of fiber fracture in damaged laminates using x-ray radiography," *J. of Comp. Tech. & Res.*, **19(1)**, pp. 10-19, 1997.

[9] R. H. Bossi and G. E. Georgeson, "Composite structure development decisions using x-ray CT measurements," *Materials Evaluation*, **53(10)**, pp. 1198-1203, 1995.

[10] P. Jezzard, C. J. Wiggins, T. A. Carpenter, L. D. Hall, J. A. Barnes, P. Jackson, and N. J. Clayden, "Demonstration of nuclear magnetic resonance imaging for void detection in carbon-fibre reinforced composites, and comparison with ultrasound methods," *J. Mat. Sci*., **27(23)**, pp. 6365-6370, 1992.

[11] Identification of a commercial product is made only to facilitate experimental reproducibility and to adequately describe experimental procedure. In no case does it imply endorsement by NIST or imply that it is necessarily the best product for the experimental procedure.

[12] J. Dunkers, K. Flynn, and R. Parnas, "A mid-infrared attenuated total internal reflection cure sensor for control of resin transfer molding of a pre-ceramic polymer," *Composites, Pt. A.*, **28(2)**, pp. 163-170, 1997.

[13] S. Ranganathan, G. Wise, F. Phelan Jr., R. Parnas, S. and Advani, *Advanced Composites X: Proceedings of the 10th Annual ASM/ESD Advanced Composites Conference and Exposition (ACCE94), ASM International*, 309(1994).

[14] T. S. Lundström, "Void formation and transport in manufacturing of polymer composites," Ph.D. Thesis, Luleå University of Technology, Luleå, Sweden, 1996.

[15] J. P. Dunkers, R. S. Parnas, C. G. Zimba, R. S. Peterson, K. M. Flynn, J. G. Fujimoto, and B. E. Bouma, "Optical coherence tomography of glass reinforced polymer composites," *Composites, Part A*, in press.

[16] F. R. Phelan, Y. Leung, and R. S. Parnas, "Modeling the microscale flow in unidirectional fibrous porous media," *Journal of Thermoplastic Composite Materials*," **7**, pp. 208-218, 1994.

[17] D. J. Bradley, D. O. Adams, and H. E. Gascoigne, "Interlaminar strains and compressive strength reductions due to nested layer waviness in composite laminates," *J. of Rein. Plas & Comp.*, **17(11)**, pp. 989-1010, 1998.

[18] E. D. Blodget , J. G. Miller, and S. M. Freeman, "Correlation of ultrasonic polar backscatter with the deply technique for assessment of impact damage in composite laminates," in *Review of Progress in Quantitative Nondestructive Evaluation*, D. O. Thompson and S. E. Chimenti, eds, pp. 1227-1238, Plenum, New York, 1986.
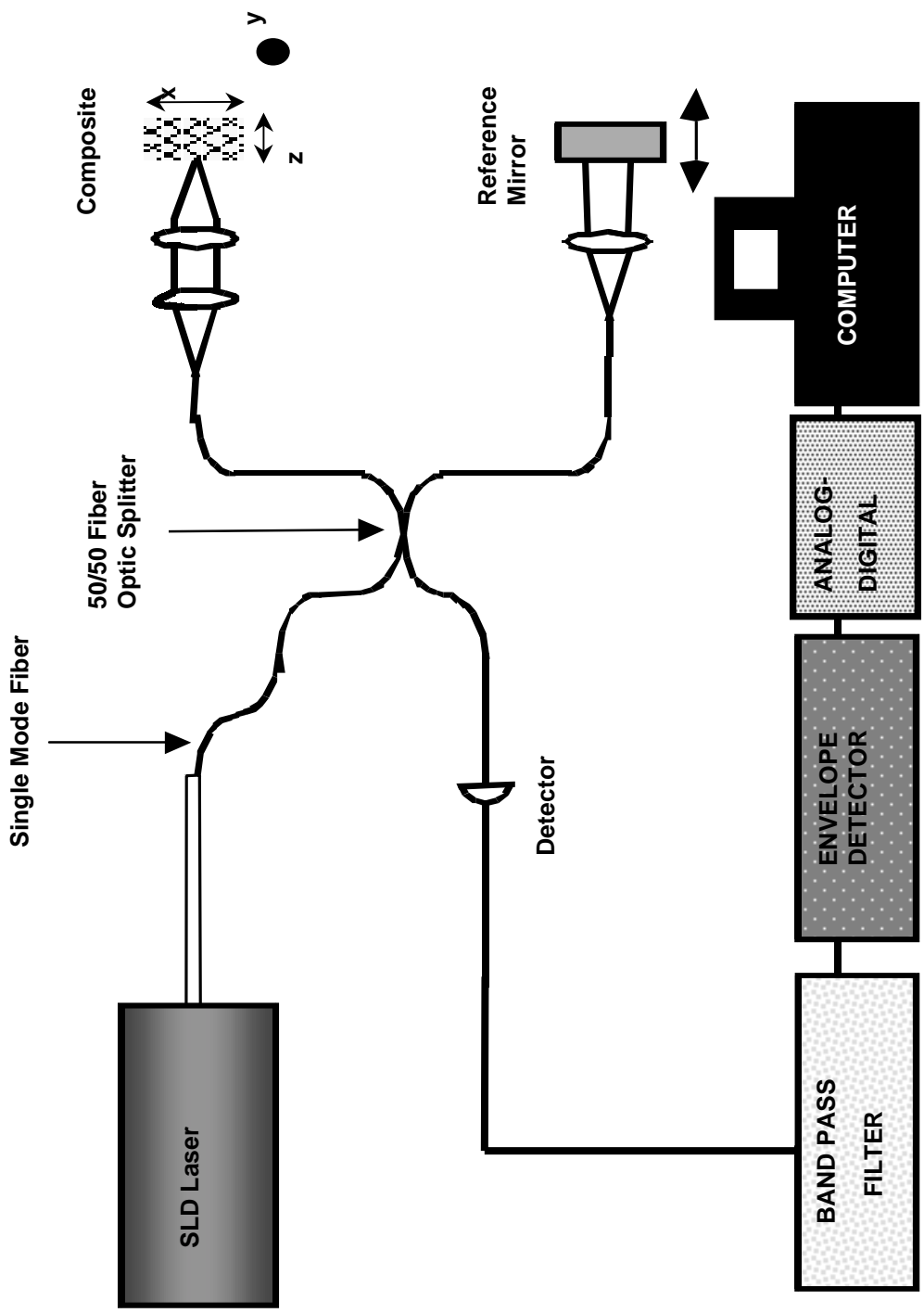
Composite

y

x

z

Single Mode Fiber

50/50 Fiber
Optic Splitter

Reference
Mirror

SLD Laser

Detector

COMPUTER

ANALOG-
DIGITAL

ENVELOPE
DETECTOR

BAND PASS
FILTER

Figure 1: Schematic representation of the solid state laser and OCT system layout
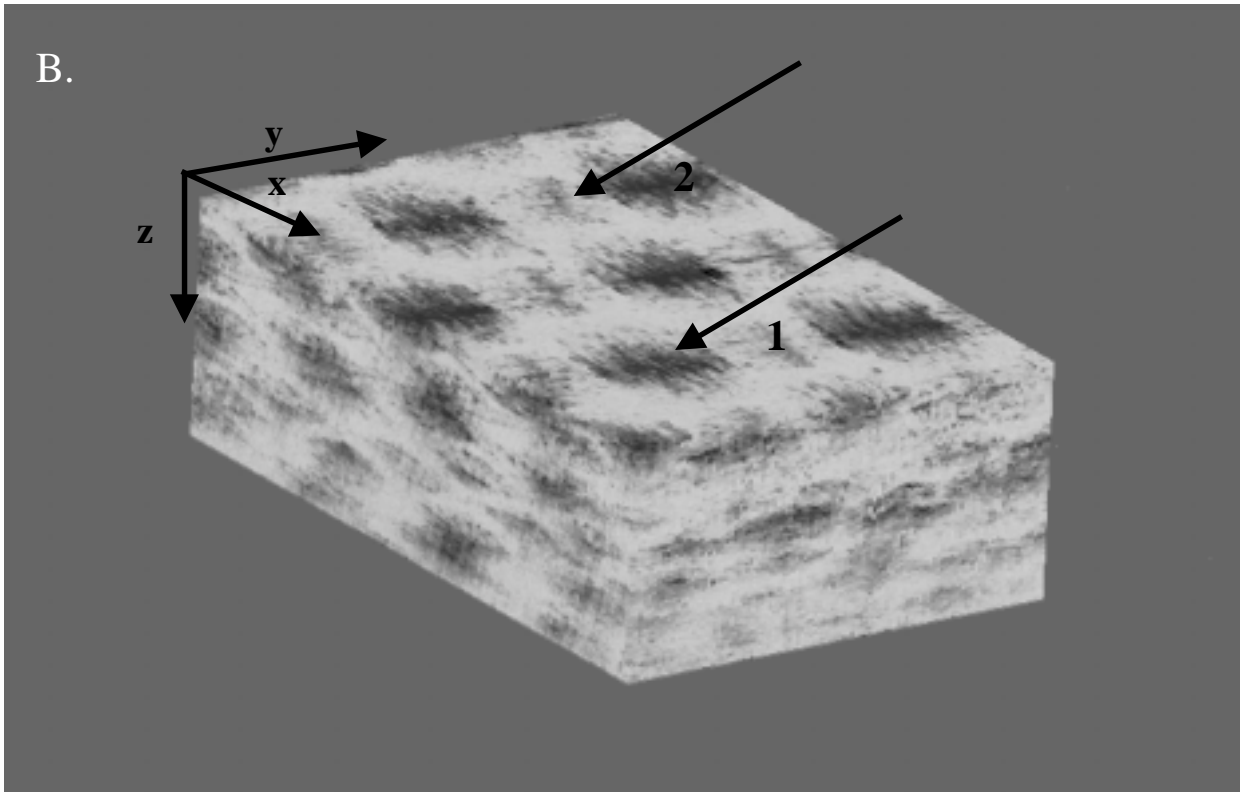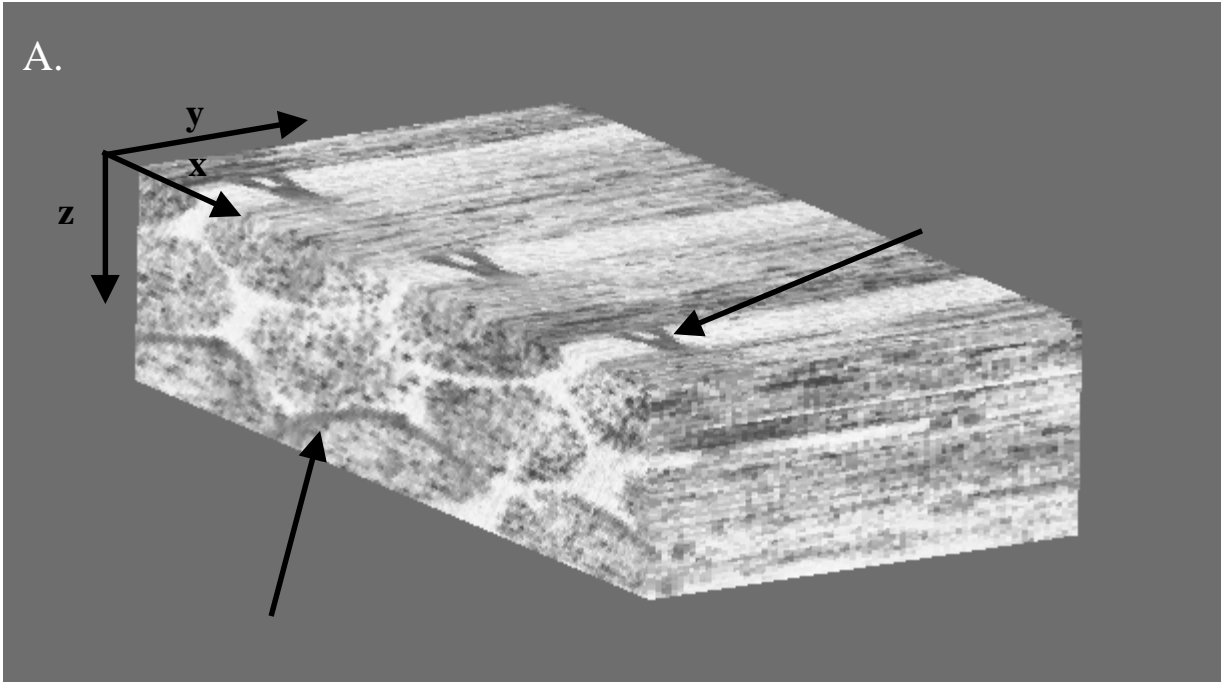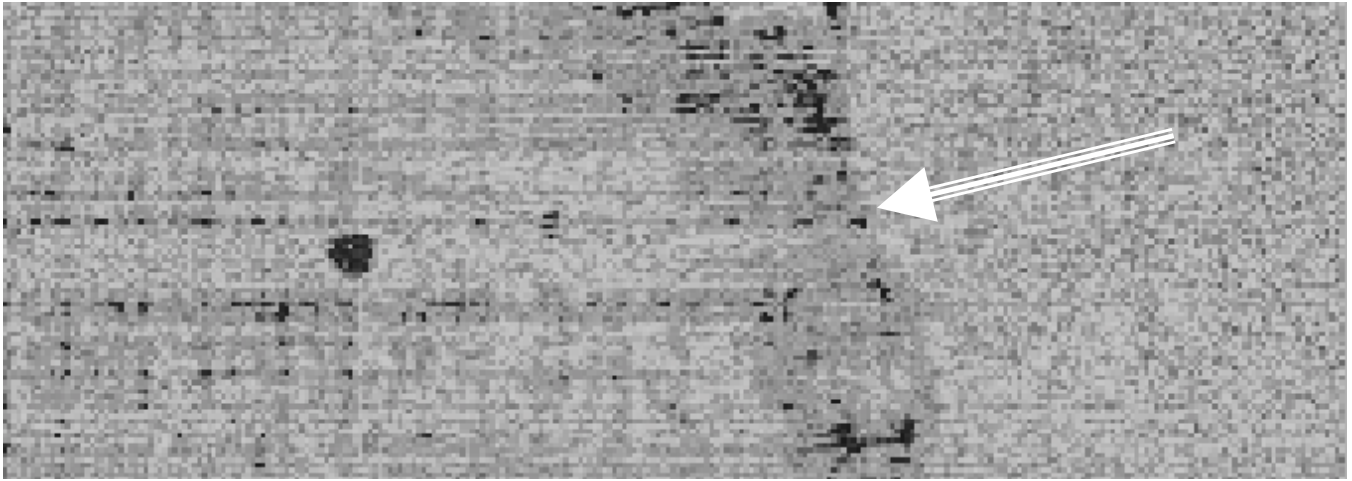
Figure 2: OCT volumetric reconstructions of an epoxy/unidirectional E-glass composite (A.) and an epoxy/0-90° woven E-glass composite (B.).
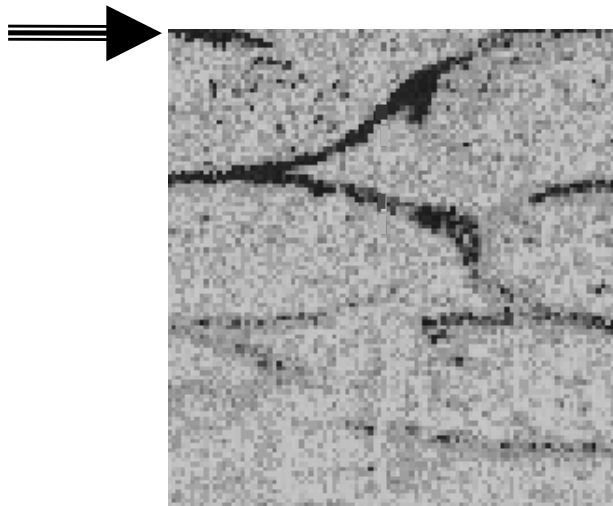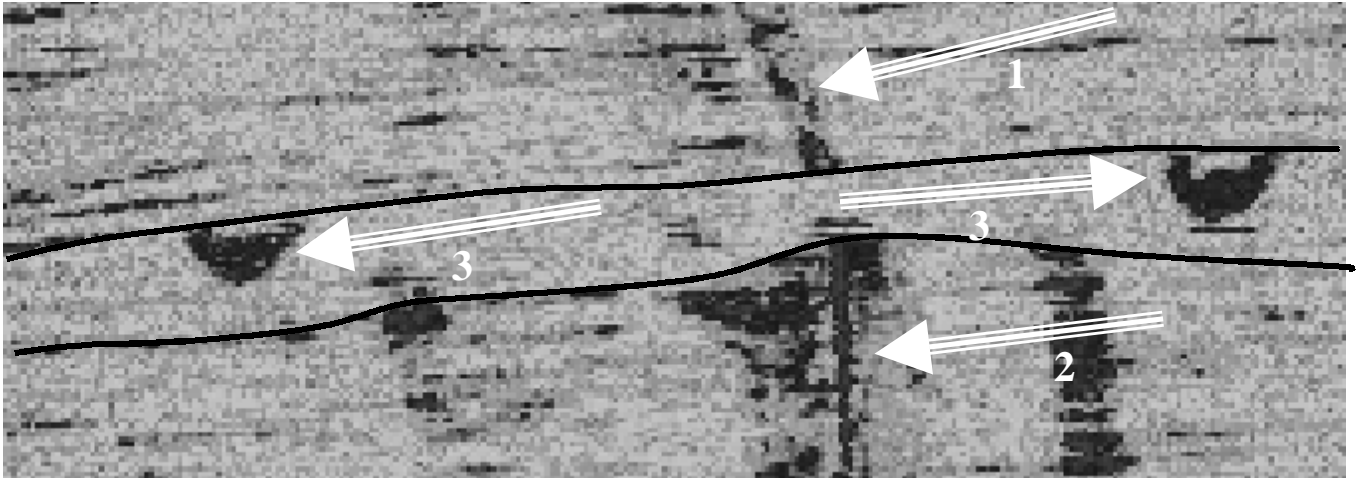
A.

B.
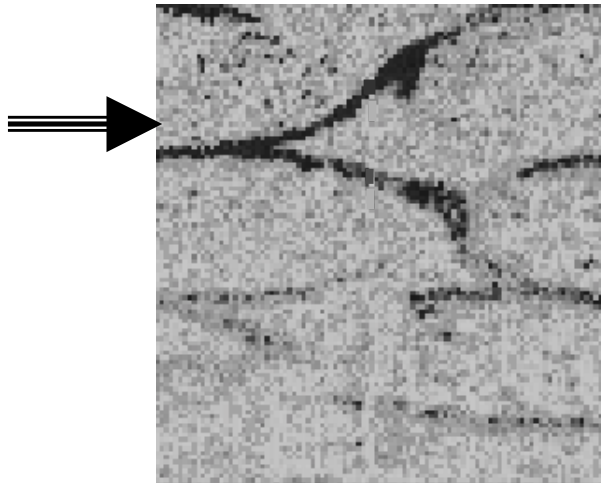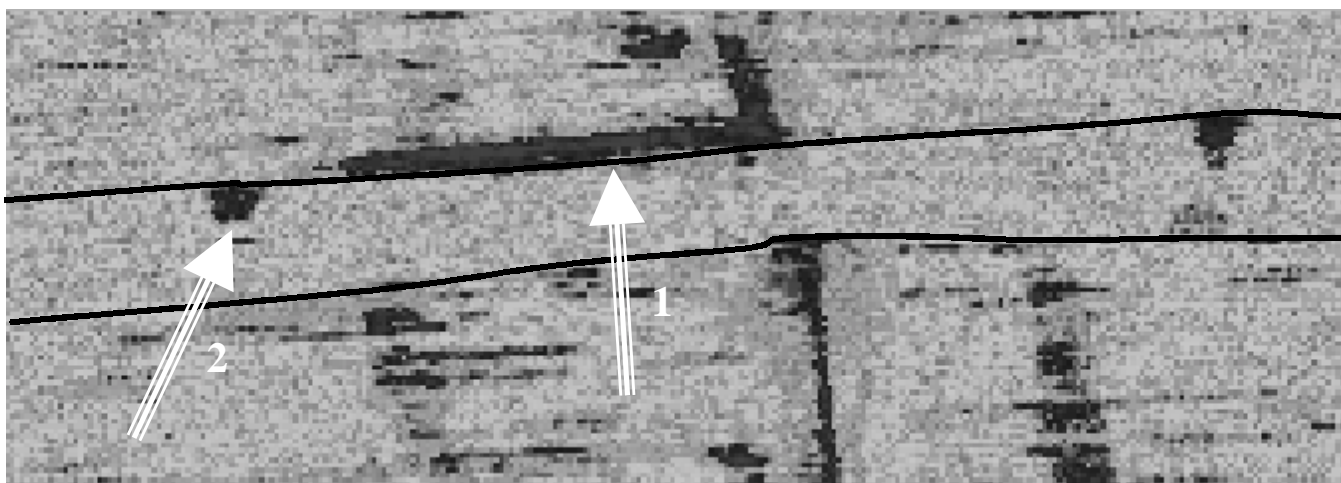

Figure 3: OCT image of impact damaged epoxy/unidirectional E-glass composite. 0 μm from surface along the x-z plane (A.). Along the y-z plane showing placement of tows via polyester stitching (B.).
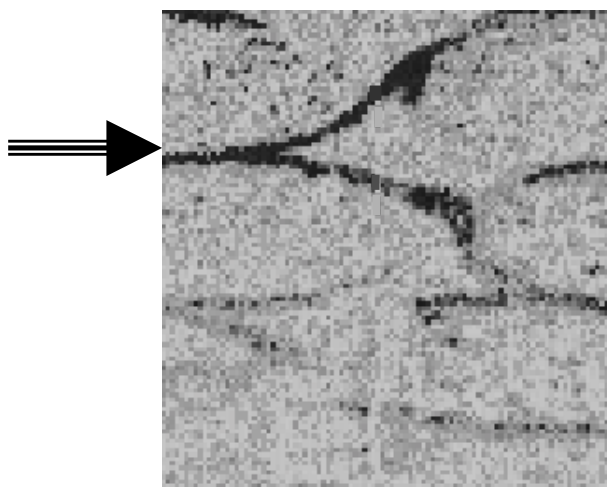
A.

B.
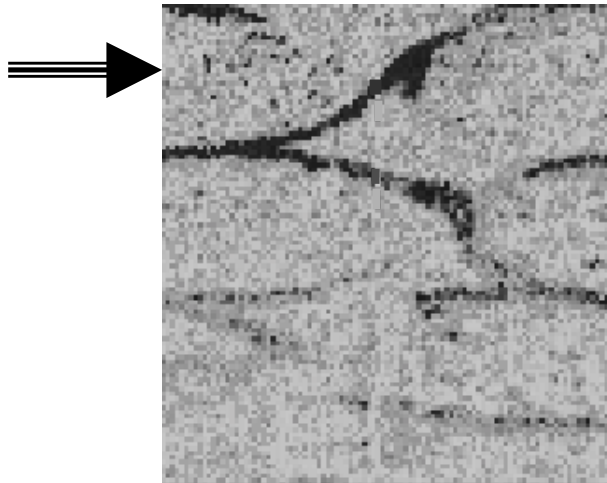
Figure 4: OCT image of impact damaged epoxy/unidirectional E-glass composite. 337 µm from surface along the x-z plane (A.). Along the y-z plane showing placement of tows via polyester stitching (B.).

A.

B.

Figure 5: OCT image of impact damaged epoxy/unidirectional E-glass composite. 460 μm from surface along the x-z plane (A.). Along the y-z plane showing placement of tows via polyester stitching (B.).
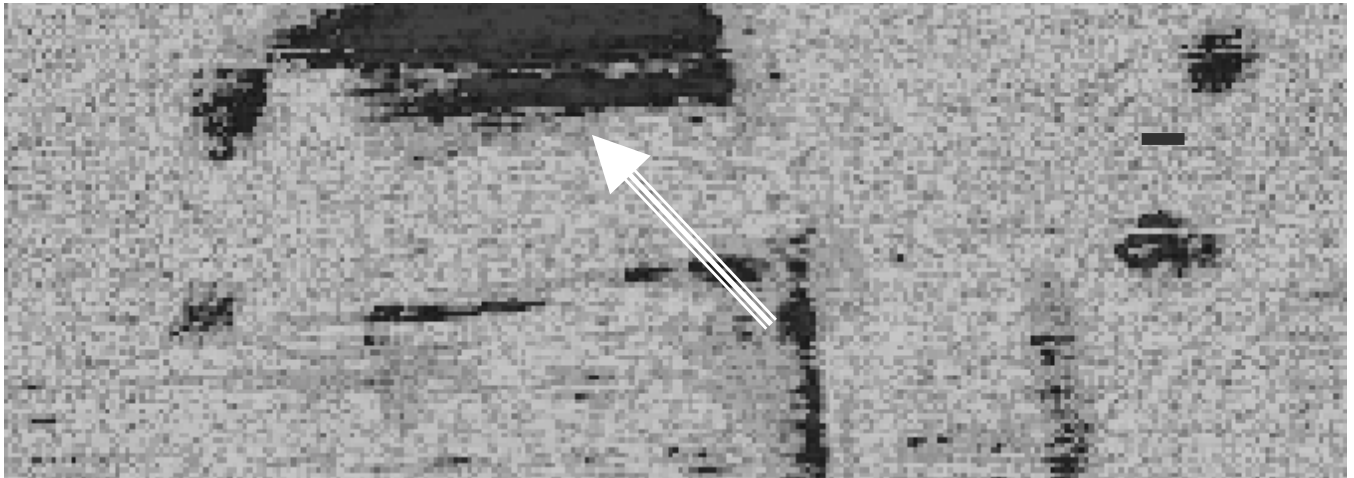
A.

B.

Figure 6: OCT image of impact damaged epoxy/unidirectional E-glass composite. 550 µm from surface along the x-z plane (A.). Along the y-z plane showing placement of tows via polyester stitching (B.).
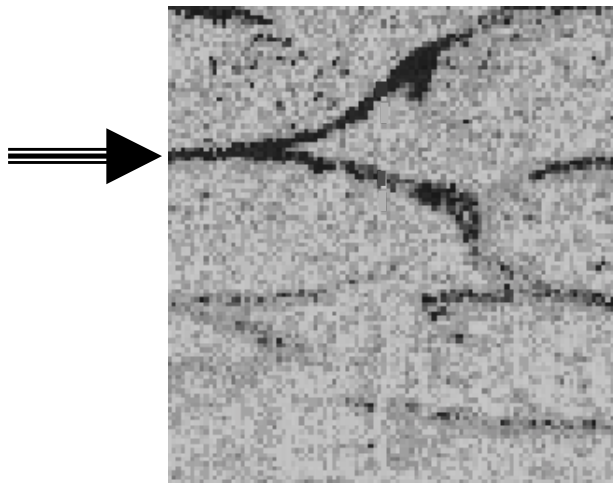
A.

B.

Figure 7: OCT image of impact damaged epoxy/unidirectional E-glass composite. 652 µm from surface along the x-z plane (A.). Along the y-z plane showing placement of tows via polyester stitching (B.).